Reflected entropy and Markov gap in noninertial frames

Jaydeep Kumar Basak,[1,2,†] Dimitrios Giataganas,[1,2,3,*] Sayid Mondal,[4,‡] and Wen-Yu Wen[4,5,§]

[1]*Department of Physics, National Sun Yat-Sen University, Kaohsiung 80424, Taiwan*
[2]*Center for Theoretical and Computational Physics, Kaohsiung 80424, Taiwan*
[3]*Physics Division, National Center for Theoretical Sciences, Taipei 10617, Taiwan*
[4]*Center for High Energy Physics and Department of Physics, Chung-Yuan Christian University, Taoyuan, Taiwan*
[5]*Leung Center for Cosmology and Particle Astrophysics, National Taiwan University, Taipei, Taiwan*

(Received 25 July 2023; accepted 27 November 2023; published 19 December 2023)

We explore the reflected entropy and the Markov gap between two modes of a free fermionic field as observed by accelerating observers. This is done for both a bipartite system, which is described by the Bell state, and tripartite systems, which are represented by the Werner and Greenberger-Horne-Zeilinger states. The reflected entropy of the fermionic modes degrades monotonically as a result of the Unruh effect, eventually reaching a nonzero minimum value in the limit of infinite acceleration. Furthermore, we show that the Markov gap exhibits monotonic behavior with regard to acceleration in all three cases. In addition, we suggest a function for reflected entropy which decreases monotonically with decreasing Unruh temperature for all states. Finally, we confirm that the reflected entropy for our system does reduce under the partial tracing of the degrees of freedom for our states.

DOI: 10.1103/PhysRevD.108.125009

I. INTRODUCTION

Entanglement has emerged as a central issue in diverse areas of theoretical and experimental physics from condensed matter physics to quantum theory of gravity. It has served as a resource of several nonlocal observables for quantum information tasks and quantum communications. A large part of entanglement studies consists of nonrelativistic systems. More recently, the understanding of entanglement has been extended in relativistic settings and has been explored in different directions. It is believed to be important from a fundamental point of view and for applications. Various experiments in quantum information theory involve observers with relativistic velocities which demand a rich theoretical understanding of the characteristics of entanglement in noninertial frames. It is known that entanglement between observers in an inertial frame remains constant. On the other hand, when relativistic noninertial motion is involved, the quantum information becomes observer dependent. A simple system to study this phenomenon is to consider the entanglement of a noninteracting massless field from the point of view of an observer who is uniformly accelerated [1]. One may assume in the inertial frame a maximally entangled pure state, whose modes are obtained from a massless scalar field, as the solution of the Klein-Gordon equation in Minkowski coordinates. To describe the state from the point of view of noninertial observers, the massless scalar field should be now considered in Rindler spacetime. A Bogoliubov transformation on the former solution in Minkowski space leads to the latter one in the Rindler spacetime [2]. An immediate consequence is that a pure state described by inertial observers becomes mixed for the uniformly accelerated observers. Following this approach, it has been found that noninertial observers see a degradation of the entanglement compared to the inertial ones. The studies have been extended to the fermionic systems [3] following a similar methodology with the solution and their transformation of the Dirac equation in different spacetimes, eventually obtaining the same qualitative results.

The ground state of a given mode for inertial observers becomes a two-mode state for accelerated observers, each one corresponding to the field observed in the two causally disconnected Rindler regions. This is due to the fact that now the state is thermal, where an information loss appears for an observer in one of the regions, since he/she needs to trace over the other region [4,5]. So far, we have reported the results of the various entanglement measures in the system under study. Nevertheless, a more appropriate, richer measure can be used for the investigation of the correlation of these types of mixed states. In the context of quantum information theory, bipartite entanglement has

*Corresponding author: dimitrios.giataganas@mail.nsysu.edu.tw
†jkb.hep@gmail.com
‡sayid.mondal@gmail.com
§wenw@cycu.edu.tw

been studied widely to understand the entanglement structure of any system. Several attempts have been made to explore the multipartite entanglement. This type of correlation has a wide range of applications in various quantum phenomena ranging from quantum gravity to quantum computation. Despite its importance, multipartite entanglement measure is still a challenging field of research in quantum information theory (see [6–9] and reference therein for recent progress).

More recently, the so-called reflected entropy has been proposed as a crucial tool to investigate the correlation of a mixed state [10]. This measure involves a canonical purification of a mixed state which is easier to obtain compared to the purification considered in the computation of the entanglement of purification. The computation of reflected entropy was introduced for a conformal field theory (CFT) based on a specific replica technique. The reflected entropy has been studied extensively in several theories and systems, for example, in [11–15] and references therein. The entanglement wedge cross section has been suggested as the holographic dual of reflected entropy in the framework of AdS/CFT correspondence. Note that the entanglement wedge cross section has also been proposed to be dual to the entanglement of purification in [16,17]. Furthermore, it was argued that the tripartite entanglement is necessary for holographic CFT states in order to respect the conjectures about the reflected entropy or entanglement of purification involving the entanglement wedge cross section [18]. These results indicate that the reflected entropy inherits some information about the multipartite entanglement by studying a two-party state.[1] Following these developments, two non-negative measures of tripartite entanglement named g and h have been proposed in [8]. The measure g is defined as the difference between the reflected entropy and the mutual information, whereas for h, it is the difference between the double of entanglement of purification and the mutual information. Furthermore, the quantity g has been explored in [21] from an information theoretic point of view where it was related to a specific Markov recovery problem, and thus, the name Markov gap was coined. A nonvanishing value of the Markov gap precludes a perfect Markov recovery map. It has been also demonstrated that the lower bound of the Markov gap in a holographic CFT state is related to the number of boundaries of the entanglement wedge cross section. Despite the success of the reflected entropy in the context of AdS/CFT duality, the monotonicity of this measure under partial tracing, which is a requirement of a good measure of correlation, has been questioned very recently in [22]. For a qutrit-qutrit-qubit system, the density matrix of a fine-tuned quantum state can violate the monotonicity of the reflected entropy for the Renyi index $\xi \in (0, 2)$.

These developments generate an intense interest to understand the reflected entropy from the viewpoint of quantum information theory. In this article, we extend these studies of fermionic systems in noninertial frames. We make use of the relationship between the Minkowski and the Rindler annihilation and creation operators of fermions with the Bogoliubov transformation in order to obtain our results. The two leading protagonists are the reflected entropy and the Markov gap considered for three different scenarios. In the first case, we have two observers, one stationary (Alice) and the other accelerating (Bob), who shared a bipartite entangled fermionic mode described by the Bell state in an inertial frame. In the second and third scenarios, there are three observers, with Alice and Charlie being stationary and Bob accelerating uniformly, who initially shared a tripartite entangled fermionic mode described by the Werner state (W state) and the Greenberger-Horne-Zeilinger (GHZ) state. We study in detail the reflected entropy for these states. To begin with, we show that reflected entropy is monotonic under partial trace for our states, which indicates that it is a good measure of correlation at least for the states in question and the acceleration of the observers we consider. Reflecting on the recent developments, this is a necessary check. As a relevant side exercise, we show that new states exist (with no acceleration involved) in higher-dimensional Hilbert spaces that violate the monotonicity of reflected entropy confirming and extending the work of [22]. Getting back to our system, we study the properties of the reflected entropy for all our states. We find a degradation of correlation between Alice and Bob due to the Unruh effect in all three scenarios. In the limit of infinite acceleration, the reflected entropy reaches a nonzero minimum value. Meanwhile, the Markov gap between Alice and Bob exhibits a monotonic behavior with respect to acceleration, and we notice that it increases for the Bell and GHZ states, whereas it decreases with acceleration for the W state. Furthermore, we define a specific dimensionless function, which we call a σ function, that depends on reflected entropy which, in all scenarios, exhibits monotonic behavior with Unruh temperature and shows interesting properties.

This paper is arranged as follows: In Sec. II, we explain the setup, defining the states and the effect of acceleration on them. These are the states we study later in this article. In Sec. III, we present the results for reflected entropy and also study its bounds in the noninertial frames. In Sec. IV, we analyze the Markov gap which indicates a specific evolution of three-party correlation. Next in Sec. V, we discuss a monotonic σ function based on reflected entropy. Finally, in Sec. VI, we summarize our results and present some of the future directions of our work. Our results of the main text are supported by three appendixes.

[1]There are other entanglement measures, i.e., three tangle [19] and π tangle [20], in the literature which are used frequently to quantify tripartite entanglement.

II. THE STATES AND THE NONINERTIAL OBSERVERS

We consider a free Dirac field in $(1+1)$-dimensional Minkowski space with coordinates $x^\mu = (t, z)$,

$$i\gamma^\mu \partial_\mu \psi - m\psi = 0, \tag{2.1}$$

where m is the particle mass, ψ is the spinor wave function, and γ^μ are the Dirac gamma matrices. This field may be expanded in terms of positive (fermions) ψ_k^+ and negative (antifermions) ψ_k^- energy solutions as

$$\psi = \int dk \left(a_k \psi_k^+ + b_k^\dagger \psi_k^-\right), \tag{2.2}$$

where k is the momentum. The Minkowski creation and annihilation operators $(a_k^\dagger, b_k^\dagger)$ and (a_k, b_k) for fermions and antifermions satisfy the anticommutation relations

$$\{a_i, a_j^\dagger\} = \{b_i, b_j^\dagger\} = \delta_{ij} \tag{2.3}$$

with all other anticommutators vanishing. The Minkowski vacuum state is given as

$$|0\rangle = \prod_{kk'} |0_k\rangle^+ |0_{k'}\rangle^-, \tag{2.4}$$

where the $\{+,-\}$ superscript on the kets indicates the fermion and antifermion vacua. Note that as $(a_k^\dagger)^2 = (b_k^\dagger)^2 = 0$, there are only two allowed states for each mode, $|0_k\rangle^+$ and $|1_k\rangle^+ = a_k^\dagger |0_k\rangle^+$ for fermions, and $|0_k\rangle^-$ and $|1_k\rangle^- = b_k^\dagger |0_k\rangle^-$ for antifermions.

In our work, we consider three distinct scenarios. In the first case, we consider two noninertial observers sharing an initially entangled bipartite fermionic field mode described by the Bell state, which is given as[2]

$$|B\rangle_{AB} = \alpha |0\rangle_A |0\rangle_B + \sqrt{1-\alpha^2}\,|1\rangle_A |1\rangle_B, \quad \alpha \in (0,1), \tag{2.5}$$

where the subscripts A and B indicate the modes associated with the observers Alice and Bob, respectively. In the second and third cases, we consider two tripartite entangled fermionic field modes represented by the Werner and GHZ states, which are given as

$$|W\rangle_{ABC} = \alpha |1\rangle_A |0\rangle_B |0\rangle_C + \alpha |0\rangle_A |0\rangle_B |1\rangle_C + \sqrt{1-2\alpha^2}\,|0\rangle_A |1\rangle_B |0\rangle_C, \quad \alpha \in \left(0, \frac{1}{\sqrt{2}}\right) \tag{2.6}$$

and

$$|\mathrm{GHZ}\rangle_{ABC} = \alpha |0\rangle_A |0\rangle_B |0\rangle_C + \sqrt{1-\alpha^2}\,|1\rangle_A |1\rangle_B |1\rangle_C, \quad \alpha \in (0,1), \tag{2.7}$$

where the subscripts A, B, and C indicate the modes associated with the observers Alice, Bob, and Charlie.

At this stage, we need to choose which of the observers is stationary and which is accelerating. For the case of bipartite state Eq. (2.5), we choose the observer Alice to be stationary carrying a detector sensitive only to mode $|n\rangle_A$, and Bob moves with uniform acceleration possessing a detector that only detects mode $|n\rangle_B$. As for the tripartite states Eqs. (2.6) and (2.7), we choose Alice and Charlie who detect mode $|n\rangle_A$ and mode $|n\rangle_C$, respectively, to be stationary, and the accelerating Bob who detects mode $|n\rangle_B$.

Rindler coordinates (τ, ξ) are appropriate to describe an observer moving with uniform acceleration in an inertial plane described by Minkowski coordinates (t, z). To describe the entire Minkowski space, two different sets of Rindler coordinates are required, which differ from each other by an overall change in sign. These sets of coordinates define two causally disconnected Rindler regions I and II that are defined as

$$\begin{aligned} t &= a^{-1} e^{a\xi} \sinh a\tau, \qquad z = a^{-1} e^{a\xi} \cosh a\tau, \quad \text{region I}, \\ t &= -a^{-1} e^{a\xi} \sinh a\tau, \qquad z = a^{-1} e^{a\xi} \cosh a\tau, \quad \text{region II}, \end{aligned} \tag{2.8}$$

where a denotes the proper acceleration of the observer Bob. The Rindler spacetime, the observers, and the regions are depicted in Fig. 1. The Rindler regions I and II are causally disconnected, and the accelerating observer in either region has no access to the other, which leads to the detection of a thermal mixed state. Henceforth, we will refer the observer in region I as Bob (B) and the observer in region II as anti-Bob ($\bar{B}$).

The Minkowski and Rindler creation and annihilation operators are related to each other through the Bogoliubov transformation as [3,23–27]

$$\begin{bmatrix} a_k \\ b_{-k}^\dagger \end{bmatrix} = \begin{bmatrix} \cos r & -e^{-i\phi} \sin r \\ e^{i\phi} \sin r & \cos r \end{bmatrix} \begin{bmatrix} c_k^I \\ d_{-k}^{II\dagger} \end{bmatrix}, \tag{2.9}$$

where (c_k^I, d_k^I) and $(c_k^{I^\dagger}, d_k^{I^\dagger})$ are annihilation and creation operators for the fermion and antifermion, respectively, in Rindler region I. In Eq. (2.9), $r = \tan^{-1} \exp(-\frac{\pi\omega}{a})$ is the acceleration parameter ranging from $0 \le r < \pi/4$ corresponding to $0 \le a < \infty$, and ω indicates the Rindler mode frequency as measured by the observer Bob with proper acceleration a. The phase ϕ in Eq. (2.9) is unimportant, and it can be absorbed in the definition of operators. The corresponding annihilation and creation operators in

[2]From now on, we will only consider the fermionic field modes, and we will also omit the superscript $\{+\}$ and subscript k on the kets.

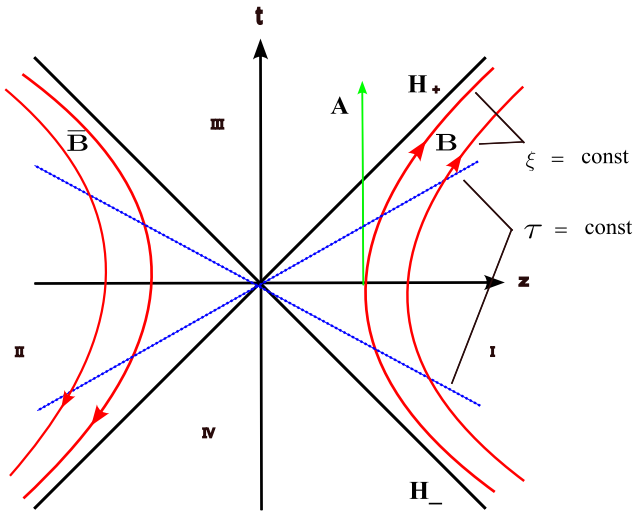

FIG. 1. Rindler spacetime diagram: The accelerating observer Bob (B) in region I and anti-Bob $\bar{B}$ in region II travel through a constant ξ hyperbola (red solid), and $\tau = \text{const}$ are lines (blue dashed) that pass through the origin. Note that time τ flows in the upward direction in region I, whereas it runs in the opposite direction in region II. The stationary observer Charlie (C) follows a similar path as Alice (A). The horizons $H_{\pm}$ are lines corresponds to $\tau = \pm\infty$.

region II are $(c_k^{II}, c_k^{II\dagger})$ and $(d_k^{II}, d_k^{II\dagger})$, respectively. Similarly, the Bogoliubov transformation that mixes antifermion modes in region I to fermion modes in region II is given as follows:

$$\begin{bmatrix} b_k \\ a_{-k}^{\dagger} \end{bmatrix} = \begin{bmatrix} \cos r & e^{-i\phi}\sin r \\ -e^{-i\phi}\sin r & \cos r \end{bmatrix} \begin{bmatrix} d_k^{I} \\ c_{-k}^{II\dagger} \end{bmatrix}. \tag{2.10}$$

By quantizing the fermionic field in the Minkowski and Rindler frames, respectively, one can relate the Minkowski particle vacuum for Bob's modes in terms of Rindler Fock states through the Bogoliubov transformations as [2,3][3]

$$|0\rangle_B = \cos r|0\rangle_B|0\rangle_{\bar{B}} + \sin r|1\rangle_B|1\rangle_{\bar{B}}, \tag{2.11}$$

and the excited state $|1\rangle_B$ is given as

$$|1\rangle_B = |1\rangle_B|0\rangle_{\bar{B}}. \tag{2.12}$$

Note that as Bob accelerates through the Minkowski vacuum $|0\rangle$, his detector detects a number of particle given by

$$\langle 0|c_k^{I\dagger}c_k^{I}|0\rangle_B = \frac{1}{1+e^{\hbar\omega/(k_B T)}}, \tag{2.13}$$

where the Unruh temperature T is related to the proper acceleration a as

$$T = \frac{a}{2\pi}. \tag{2.14}$$

A. Bell state

The bipartite fermionic field modes described by the Bell state (2.5) may be expressed by employing Eqs. (2.11) and (2.12) as

$$\begin{aligned} |B\rangle_{AB\bar{B}} = {} & \alpha\cos r|000\rangle_{AB\bar{B}} + \alpha\sin r|011\rangle_{AB\bar{B}} \\ & + \sqrt{1-\alpha^2}|110\rangle_{AB\bar{B}}, \end{aligned} \tag{2.15}$$

where we have denoted $|l\rangle_A|m\rangle_B|n\rangle_{\bar{B}} = |lmn\rangle_{AB\bar{B}}$, and for simplicity, we will henceforth denote $|lmn\rangle_{AB\bar{B}}$ as $|lmn\rangle$. The mixed density matrices for Alice-Bob (AB), Alice–anti-Bob $(A\bar{B})$, and Bob–anti-Bob $(B\bar{B})$ are given as follows:

$$\begin{aligned} \rho_{AB}^{(B)} &= \alpha^2\cos^2 r|00\rangle\langle 00| + \alpha\sqrt{1-\alpha^2}\cos r(|00\rangle\langle 11| + |11\rangle\langle 00|) + \alpha^2\sin^2 r|01\rangle\langle 01| + (1-\alpha^2)|11\rangle\langle 11|, \\ \rho_{A\bar{B}}^{(B)} &= \alpha^2\cos^2 r|00\rangle\langle 00| + \alpha^2\sin^2 r|01\rangle\langle 01| + \alpha\sqrt{1-\alpha^2}\sin r(|01\rangle\langle 10| + |10\rangle\langle 01|) + (1-\alpha^2)|10\rangle\langle 10|, \\ \rho_{B\bar{B}}^{(B)} &= \alpha^2\cos^2 r|00\rangle\langle 00| + \alpha^2\cos r\sin r(|00\rangle\langle 11| + |11\rangle\langle 00|) + (1-\alpha^2)|10\rangle\langle 10| + \alpha^2\sin^2 r|11\rangle\langle 11|, \end{aligned} \tag{2.16}$$

where the superscript refers to the state, in this case the Bell state. Similarly, the density matrices for Alice, Bob, and anti-Bob, respectively, are $\rho_A^{(B)}$, $\rho_B^{(B)}$, and $\rho_{\bar{B}}^{(B)}$. They can be found as

$$\begin{aligned} \rho_A^{(B)} &= \alpha^2|0\rangle\langle 0| + (1-\alpha^2)|1\rangle\langle 1|, \\ \rho_B^{(B)} &= \alpha^2\cos^2 r|0\rangle\langle 0| + (1-\alpha^2\cos^2 r)|1\rangle\langle 1|, \\ \rho_{\bar{B}}^{(B)} &= (1-\alpha^2\sin^2 r)|0\rangle\langle 0| + \alpha^2\sin^2 r|1\rangle\langle 1|. \end{aligned} \tag{2.17}$$

[3]Note that we have employed the single-mode approximation as described in [3].

B. Werner state

The tripartite entangled fermionic mode described by the W state in Eq. (2.6) may be express as follows by employing Eqs. (2.11) and (2.12):

$$|W\rangle_{ABC} = \alpha\cos r|1000\rangle_{AB\bar{B}C} + \alpha\sin r|1110\rangle_{AB\bar{B}C} + \alpha\cos r|0001\rangle_{AB\bar{B}C} + \alpha\sin r|0111\rangle_{AB\bar{B}C} + \sqrt{1-2\alpha^2}|0100\rangle_{AB\bar{B}C}. \tag{2.18}$$

The density matrices of AB, $A\bar{B}$, and $B\bar{B}$ are given as

$$\begin{aligned}
\rho_{AB}^{(W)} &= \alpha^2\cos^2 r|00\rangle\langle 00| + ((1-2\alpha^2) + \alpha^2\sin^2 r)|01\rangle\langle 01| + \alpha\sqrt{1-2\alpha^2}\cos r(|10\rangle\langle 01| + |01\rangle\langle 10|) \\
&\quad + \alpha^2\cos^2 r|10\rangle\langle 10| + \alpha^2\sin^2 r|11\rangle\langle 11|, \\
\rho_{A\bar{B}}^{(W)} &= ((1-2\alpha^2) + \alpha^2\cos^2 r)|00\rangle\langle 00| + \alpha^2\sin^2 r|01\rangle\langle 01| + \alpha\sqrt{1-2\alpha^2}\sin r(|00\rangle\langle 11| + |11\rangle\langle 00|)| \\
&\quad + \alpha^2\cos^2 r|10\rangle\langle 10| + \alpha^2\sin^2 r|11\rangle\langle 11|, \\
\rho_{B\bar{B}}^{(W)} &= 2\alpha^2\cos^2 r|00\rangle\langle 00| + 2\alpha^2\cos r\sin r(|00\rangle\langle 11| + |11\rangle\langle 00|) + 2\alpha^2\sin^2 r|11\rangle\langle 11| + (1-2\alpha^2)|10\rangle\langle 10|,
\end{aligned} \tag{2.19}$$

while the density matrices of A, B, and $\bar{B}$ are

$$\begin{aligned}
\rho_A^{(W)} &= (1-\alpha^2)|0\rangle\langle 0| + \alpha^2|1\rangle\langle 1|, \\
\rho_B^{(W)} &= 2\alpha^2\cos^2 r|0\rangle\langle 0| + (1-2\alpha^2\cos^2 r)|1\rangle\langle 1|, \\
\rho_{\bar{B}}^{(W)} &= (1-2\alpha^2\sin^2 r)|0\rangle\langle 0| + 2\alpha^2\sin^2 r|1\rangle\langle 1|.
\end{aligned} \tag{2.20}$$

C. Greenberger-Horne-Zeilinger state

By employing Eqs. (2.11) and (2.12), the GHZ state Eq. (2.7) may further be expressed as

$$|\mathrm{GHZ}\rangle_{ABC} = \alpha\cos r|0000\rangle_{AB\bar{B}C} + \alpha\sin r|0110\rangle_{AB\bar{B}C} + \sqrt{1-\alpha^2}|1101\rangle_{AB\bar{B}C}. \tag{2.21}$$

The density matrices of AB, $A\bar{B}$, and $B\bar{B}$ are as follows:

$$\begin{aligned}
\rho_{AB}^{(\mathrm{GHZ})} &= \alpha^2\cos^2 r|00\rangle\langle 00| + \alpha^2\sin^2 r|01\rangle\langle 01| + (1-\alpha^2)|11\rangle\langle 11|, \\
\rho_{A\bar{B}}^{(\mathrm{GHZ})} &= \alpha^2\cos^2 r|00\rangle\langle 00| + \alpha^2\sin^2 r|01\rangle\langle 01| + (1-\alpha^2)|10\rangle\langle 10|, \\
\rho_{B\bar{B}}^{(\mathrm{GHZ})} &= \alpha^2\cos^2 r|00\rangle\langle 00| + \alpha^2\cos r\sin r(|00\rangle\langle 11| + |11\rangle\langle 00|) + (1-\alpha^2)|10\rangle\langle 10| + \alpha^2\sin^2 r|11\rangle\langle 11|,
\end{aligned} \tag{2.22}$$

while the density matrices of A, B, and $\bar{B}$ read

$$\begin{aligned}
\rho_A^{(\mathrm{GHZ})} &= \alpha^2|0\rangle\langle 0| + (1-\alpha^2)|1\rangle\langle 1|, \\
\rho_B^{(\mathrm{GHZ})} &= \alpha^2\cos^2 r|0\rangle\langle 0| + (1-\alpha^2\cos^2 r)|1\rangle\langle 1|, \\
\rho_{\bar{B}}^{(\mathrm{GHZ})} &= (1-\alpha^2\sin^2 r)|0\rangle\langle 0| + \alpha^2\sin^2 r|1\rangle\langle 1|.
\end{aligned} \tag{2.23}$$

III. REFLECTED ENTROPY

In this section, we study the reflected entropy between the observers Alice-Bob (AB), Alice–anti-Bob ($A\bar{B}$), and Bob–anti-Bob ($B\bar{B}$) for the Bell state given by Eq. (2.15), W state given by Eq. (2.18), and GHZ state given by Eq. (2.21), respectively. Before delving into the details of the computation, we briefly review reflected entropy in quantum information theory. To begin with, we consider a bipartite density matrix ρ_{AB} in a Hilbert space $\mathcal{H}_A \otimes \mathcal{H}_B$, where $\mathcal{H}_A$ and $\mathcal{H}_B$ are Hilbert spaces associated with the subsystems A and B, respectively. The entanglement entropy of the subsystem A is defined as the von Neumann entropy of the reduced density matrix $\rho_A = \mathrm{Tr}_B\rho_{AB}$ as

$$S(A) = -\mathrm{Tr}(\rho_A\log\rho_A). \tag{3.1}$$

The mutual information, which measures the total correlation between the subsystems A and B, is defined as

$$I(A:B) = S(A) + S(B) - S(AB), \tag{3.2}$$

which is symmetric in A and B. As mentioned in the Introduction, for mixed states the entanglement entropy is not the most appropriate entanglement measure, and other mixed state entanglement measures are to be used. Note that any mixed state ρ_{AB} in quantum information theory may be expressed as a sum of pure states

$$\rho_{AB} = \sum_a p_a \rho_{AB}^{(a)}, \qquad \rho_{AB}^{(a)} = |\phi_a\rangle\langle\phi_a|, \tag{3.3}$$

where $|\phi_a\rangle$ is an orthonormal basis of $\mathcal{H}_A \otimes \mathcal{H}_B$, and eigenvalues p_a are non-negative $0 \leq p_a \leq 1$. We construct the Schmidt decomposition of $|\phi_a\rangle$ by choosing appropriate bases $|i_a\rangle_A \in \mathcal{H}_A$ and $|i_b\rangle_B \in \mathcal{H}_b$ as

$$|\phi_a\rangle = \sum_i \sqrt{l_a^i}\, |i_a\rangle_A |i_a\rangle_B, \tag{3.4}$$

where l_a^i is a non-negative quantity with the normalization $\sum_i l_a^i = 1$. By using Eq. (3.4), the density matrix Eq. (3.3) may be expressed as

$$\rho_{AB} = \sum_{a,i,j} p_a \sqrt{l_a^i l_a^j} |i_a\rangle_A |i_a\rangle_B \langle j_a|_A \langle j_a|_B. \tag{3.5}$$

We now interpret $\langle j_a|_A$ and $\langle j_a|_B$ as states $|j_a\rangle_{A^\star}$ and $|j_a\rangle_{B^\star}$ on Hilbert spaces $\mathcal{H}_A^\star$ and $\mathcal{H}_B^\star$, respectively, and define a pure state $|\sqrt{\rho_{AB}}\rangle \in \mathcal{H}_A \otimes \mathcal{H}_B \otimes \mathcal{H}_A^\star \otimes \mathcal{H}_B^\star$ as

$$|\sqrt{\rho_{AB}}\rangle = \sum_{a,i,j} \sqrt{p_a l_a^i l_a^j}\, |i_a\rangle_A |i_a\rangle_B |j_a\rangle_{A^\star} |j_a\rangle_{B^\star}. \tag{3.6}$$

This state $|\sqrt{\rho_{AB}}\rangle$ is known as the purification of the state ρ_{AB}. The reflected entropy between A and B for ρ_{AB} is defined as the von Neumann entropy of $\rho_{AA^\star} = \mathrm{Tr}_{BB^\star} |\sqrt{\rho_{AB}}\rangle\langle\sqrt{\rho_{AB}}|$, which is given as [10,28–31]

$$S_R(A:B) = -\mathrm{Tr}_{AA^\star}[\rho_{AA^\star} \log \rho_{AA^\star}]. \tag{3.7}$$

It is interesting to note that the reflected entropy is upper bounded by $\min\{2S_A, 2S_B\}$ and lower bounded by the mutual information $I(A:B)$ as

$$\min\{2S_A, 2S_B\} \geq S_R(A:B) \geq I(A:B). \tag{3.8}$$

For any tripartite pure state, the reflected entropy satisfies the polygamy inequality (see Appendix B for details), which is given as

$$S_R(A:B) + S_R(A:C) \geq S_R(A:BC). \tag{3.9}$$

Apart from these, reflected entropy can also distinguish isospectral density matrices [32]. One example of such density matrices is

$$\rho_1 = \frac{1}{3}\begin{pmatrix} 1 & 0 & 0 & 0 \\ 0 & 1 & 1 & 0 \\ 0 & 1 & 1 & 0 \\ 0 & 0 & 0 & 0 \end{pmatrix}, \qquad \rho_2 = \frac{1}{3}\begin{pmatrix} 1 & 0 & 0 & 0 \\ 0 & 0 & 0 & 0 \\ 0 & 0 & 0 & 0 \\ 0 & 0 & 0 & 2 \end{pmatrix}, \tag{3.10}$$

where ρ_1 and ρ_2 can be written in the basis $\{|00\rangle, |01\rangle, |10\rangle, |11\rangle\}$ by tracing out one party from a W state $|W\rangle_{ABC} = \frac{1}{\sqrt{3}}(|100\rangle + |010\rangle + |001\rangle)$ and GHZ state $|\mathrm{GHZ}\rangle_{ABC} = \frac{1}{\sqrt{3}}(|000\rangle + \sqrt{2}|111\rangle)$, respectively. For example, in this case one can compute $S_R(\rho_1) = 1.49$ and $S_R(\rho_2) = 0.92$, which clearly distinguishes these two isospectral density matrices.

We now turn to the computation of reflected entropy for the bipartite and tripartite fermionic field mode as described in Eqs. (2.5)–(2.7). To compute reflected entropy $S_R(A:B)$, $S_R(A:\bar{B})$, and $S_R(B:\bar{B})$ between AB, $A\bar{B}$, and $B\bar{B}$, we first construct the canonically purified states $|\sqrt{\rho_{AB}}\rangle$, $|\sqrt{\rho_{A\bar{B}}}\rangle$, and $|\sqrt{\rho_{B\bar{B}}}\rangle$ by doubling the Hilbert space as mentioned in Eq. (3.6). Now the reflected entropies $S_R(A:B)$, $S_R(A:\bar{B})$, and $S_R(B:\bar{B})$ are obtained by using Eq. (3.7) for the Bell, W, and GHZ states (see Appendix A for details).

Note that in the inertial frame $r = 0$ and $\alpha = \frac{1}{\sqrt{2}}$ correspond to the case of the maximally entangled Bell and GHZ state, and $\alpha = \frac{1}{\sqrt{3}}$ for the maximally entangled W state. In Figs. 2(a)–2(c), we plot $S_R(A:B)$, $S_R(A:\bar{B})$, and $S_R(B:\bar{B})$ as a function of the acceleration r for fixed α for the Bell, W, and GHZ states, respectively. We notice that $S_R(A:B)$ decreases, whereas $S_R(A:\bar{B})$ increases due to the Unruh effect for all three cases. Furthermore, in the infinite acceleration limit they both reach the same nonvanishing final value, which indicates that the observers B and $\bar{B}$ become indistinguishable at this limit. We notice that as the correlation between AB decreases, the correlation between $A\bar{B}$ grows, which is due to the correlation sharing. Indeed, this phenomenon has also been observed for other entanglement measures as well, e.g., entanglement negativity [3]. On the other hand, $S_R(B:\bar{B})$ increases monotonically starting from zero at $r = 0$ culminating to a final nonzero value in the infinite acceleration limit where $r = \frac{\pi}{4}$.

Let us now briefly discuss some of the recent developments which raised a concern on the generic validity and applicability of the reflected entropy as a correlation measure in quantum information theory. It has been recently noticed [22] that in a qutrit-qutrit-qubit system there exist quantum states which violate the monotonicity of reflected entropy under the operation of partial trace. Nevertheless, it remains an important quantity in the context of holography where the entanglement wedge cross section is considered a bulk dual of reflected entropy [10]. Therefore, utilizing the

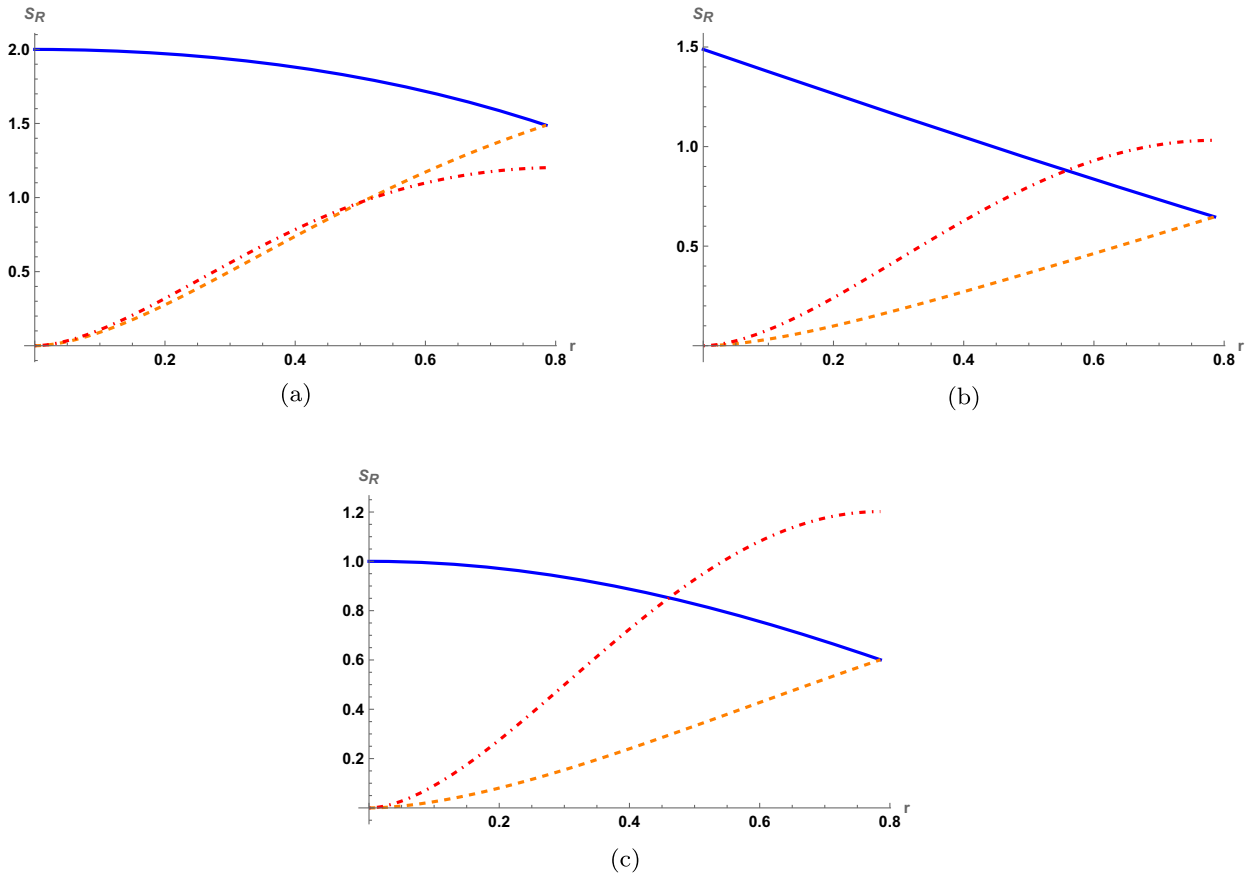

FIG. 2. Reflected entropy for the Bell, Werner, and GHZ states is plotted as a function of the acceleration. (a) Bell state: $S_R(A:B)$ (blue solid curve), $S_R(A:\bar{B})$ (orange dashed curve), and $S_R(B:\bar{B})$ (red dot-dashed curve). In all plots that follow for the Bell state, α is fixed to its maximally entangled value for the state unless otherwise stated. (b) W state: $S_R(A:B)$ (blue solid curve), $S_R(A:\bar{B})$ (orange dashed curve), and $S_R(B:\bar{B})$ (red dot-dashed curve). In all plots that follow for W state, α is fixed to its maximally entangled value for the state unless otherwise stated. (c) GHZ state: $S_R(A:B)$ (blue solid curve), $S_R(A:\bar{B})$ (orange dashed curve), and $S_R(B:\bar{B})$ (red dot-dashed curve). In all plots that follow for the GHZ state, α is fixed to its maximally entangled value for the state unless otherwise stated.

nesting property of the entanglement wedge, it can be argued that reflected entropy in holographic CFT does not suffer from nonmonotonicity [10,33]. However, for our states in this work it is essential to confirm that the reflected entropy does reduce under the partial tracing of the degrees of freedom.

As a side development to this task, we confirm and extend the work of [22] by showing that there exists another three-party state in the Hilbert space $\mathcal{H}_A \otimes \mathcal{H}_B \otimes \mathcal{H}_C = \mathbb{C}^4 \otimes \mathbb{C}^3 \otimes \mathbb{C}^2$ which violates the monotonicity of the ξth Renyi reflected entropy in the domain $\xi \in (0, 2)$,

$$\rho_{ABC} = \frac{1}{6a+2b}[a(|000\rangle\langle 000| + |110\rangle\langle 110| + |200\rangle\langle 000| + |210\rangle\langle 110| + |300\rangle\langle 000| + |310\rangle\langle 110|) + b(|020\rangle\langle 020| + |121\rangle\langle 121|)]. \tag{3.11}$$

In the above expression, a and b are two parameters which can be treated as classical probabilities. Using this state in Eq. (3.11), one can compute ξth Renyi reflected entropy and check the monotonicity under partial trace. It is observed that for some fixed range of parameters a and b, the quantity $S_R^{\xi}(A:BC) - S_R^{\xi}(A:B)$ becomes negative [Fig. 3(a)]. It is easy to check the conditions numerically, which yields that a should be larger than b. Similar to [22], increasing the value of $\frac{a}{b}$ pushes the region of violation toward $\xi = 2$. Furthermore, for a fixed value of ξ, it can be observed in Fig. 3(b) that the violation of monotonicity occurs at different values of the ratio $p = \frac{a}{b}$. The state Eq. (3.11) can be generalized for Hilbert space with arbitrary dimensions, i.e., $\mathcal{H}_A \otimes \mathcal{H}_B \otimes \mathcal{H}_C = \mathbb{C}^{n+1} \otimes \mathbb{C}^{m+1} \otimes \mathbb{C}^2$ where violation of monotonicity is observed for Rényi reflected entropy as we show in Appendix C. For the states considered in this study, we are able to confirm that the reflected entropy does reduce under the partial tracing of the degrees of freedom. We include some representative results in Appendix C. Consequently, we argue that reflected entropy is a good correlation measure for our states and the noninertial observers in our setup.

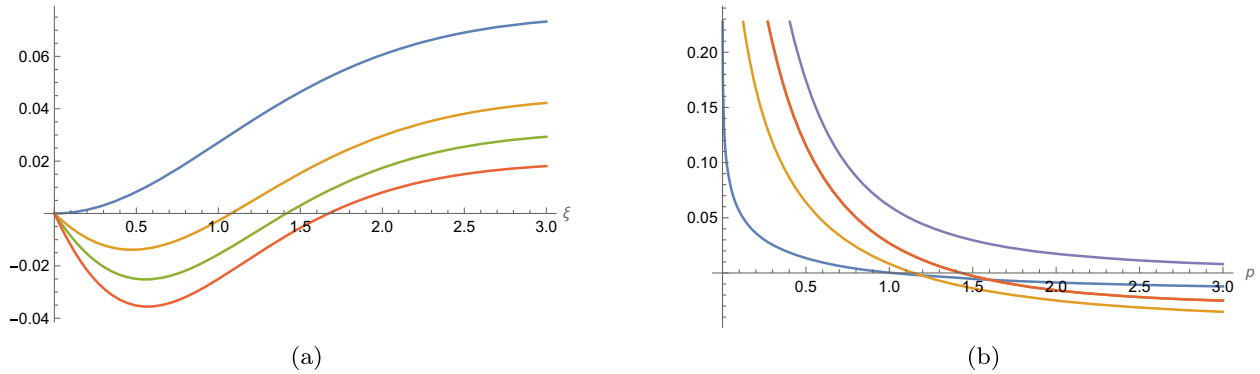

(a) (b)

FIG. 3. Monotonicity of Renyi reflected entropy under partial tracing for the state in Eq. (3.11). (a) $S_R^{\xi}(A:BC) - S_R^{\xi}(A:B)$ vs ξ. Here, $a = 0.5$ (blue), $a = 0.75$ (orange), $a = 1$ (green), $a = 1.5$ (red), and $b = 0.5$. (b) $S_R^{\xi}(A:BC) - S_R^{\xi}(A:B)$ vs p. Here, $\xi = 0.1$ (blue), $\xi = 0.5$ (orange), $\xi = 1$ (red), and $\xi = 2$ (violet).

A. Bounds of reflected entropy

In Figs. 4–6, we provide an illustrative representation of the upper and lower bounds followed by $S_R(A:B)$ as mentioned in Eq. (3.8) for the Bell, Werner, and GHZ states, respectively. For the case of the Bell state, the density matrix ρ_{AB} at $r = 0$ is pure and entangled; hence, reflected entropy $S_R(A:B)$ saturates both upper and lower bounds. Interestingly, increasing r induces tripartite entanglement into the system, which leads to the nonsaturation of the bound depicted in Fig. 4(a). In Fig. 4(b), we observe that for $\alpha = 0$ and $\alpha = 1$ both the bounds are saturated as expected, and near $\alpha = 0$, $S_R(A:B)$ (blue solid curve) follows closer to $I(A:B)$ (red dot-dashed curve), whereas close to $\alpha = 1$, it follows closer to $\min\{2S_A, 2S_B\}$ (orange dashed curve). We notice the clear shift of dominance between $\min\{2S_A, 2S_B\}$ (orange dashed curve) close to $\alpha \simeq 0.8$ from $2S_A$ to $2S_B$, where the exact value α where this happens depends on the parameters we choose for the state.

On the other hand, for the W state, ρ_{AB} at $r = 0$ is mixed and entangled, and as a result, none of the bounds are saturated, indicating the existence of tripartite entanglement which increases with r Fig. 5(a). In Fig. 5(b), we see that for $\alpha = 0$ both bounds are saturated, and at $\alpha = 1$ only the lower bound is saturated. We also observe that, unlike the behavior of the Bell state, the W state's $S_R(A:B)$ (blue solid curve) near $\alpha = 0$ follows close the $\min\{2S_A, 2S_B\}$ (orange dashed curve) whereas close to $\alpha = 1/\sqrt{2}$, it comes closer to the $I(A:B)$ (red dot-dashed curve). Furthermore, we observe a change of dominance in $\min\{2S_A, 2S_B\}$ from $2S_A$ to $2S_B$ near $\alpha \simeq .6$, as in the previous case. As for the GHZ state, at $r = 0$ the density matrix ρ_{AB} is mixed and separable; hence, only the lower bound is saturated. With increasing r, the reflected entropy $S_R(A:B)$ (blue solid curve) decreases, and none of the bounds are saturated at large r, as can be seen in Fig. 6(a). This refers to the existence of the tripartite entanglement at finite r. When $S_R(A:B)$ is plotted as a function of α at a fixed r, we observe that both bounds are saturated at $\alpha = 0$ and $\alpha = 1$ presented in Fig. 6(b). Notice the clear change of dominance of $\min\{2S_A, 2S_B\}$ (orange dashed) near $\alpha \simeq 0.8$ from $2S_A$ to $2S_B$.

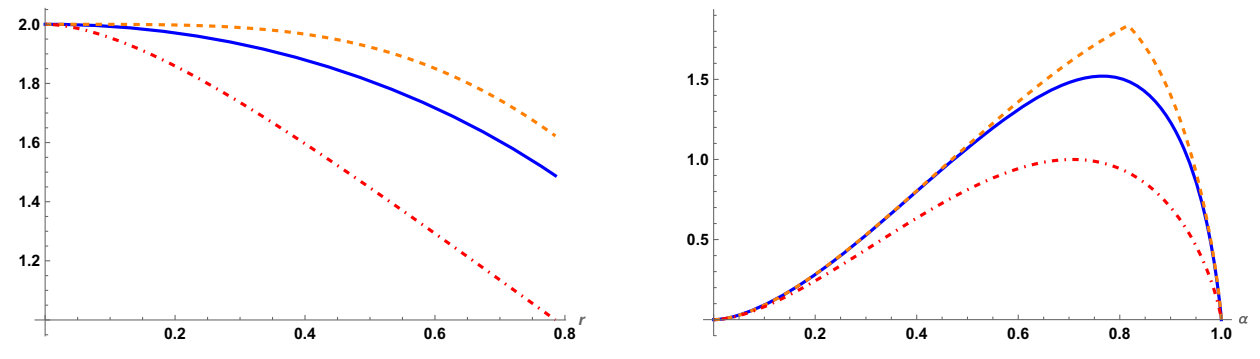

(a) (b)

FIG. 4. (a) Reflected entropy $S_R(A:B)$ for the maximally entangled Bell state as function of r is compared with its upper and lower bounds. (b) Reflected entropy $S_R(A:B)$ as a function of α for $r = \frac{\pi}{4}$ is compared with its upper and lower bounds. (a) $S_R(A:B)$ (blue solid curve), $\min\{2S_A, 2S_B\}$ (orange dashed curve), $I(A:B)$ (red dot-dashed). (b) $S_R(A:B)$ (blue solid curve), $\min\{2S_A, 2S_B\}$ (orange dashed curve), $I(A:B)$ (red dot-dashed).

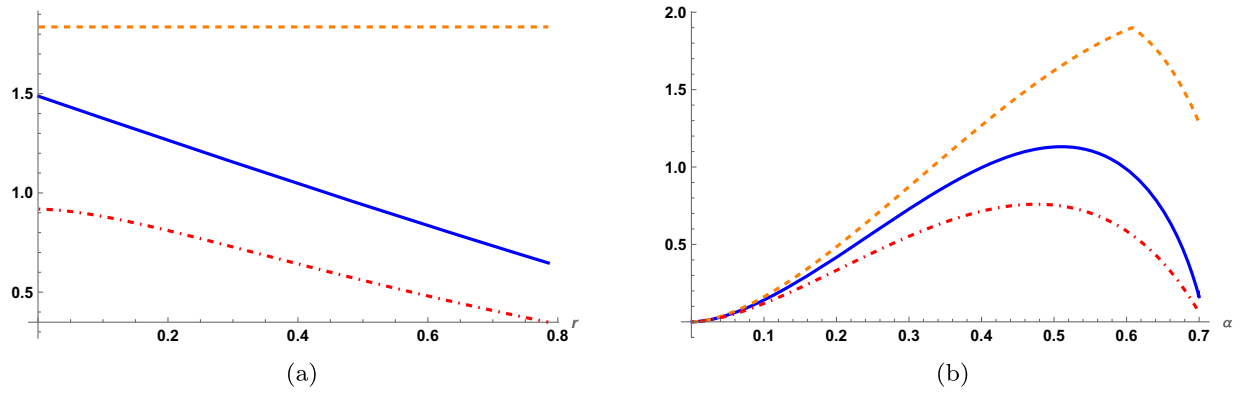

FIG. 5. (a) The reflected entropy $S_R(A:B)$ for the maximally entangled W state as function of r is compared with its upper and lower bounds. (b) Reflected entropy $S_R(A:B)$ as a function of α for $r = \frac{\pi}{8}$ is compared with its upper and lower bounds. $S_R(A:B)$ (blue solid curve), $\min\{2S_A, 2S_B\}$ (orange dashed curve), $I(A:B)$ (red dot-dashed curve). $S_R(A:B)$ (blue solid curve), $\min\{2S_A, 2S_B\}$ (orange dashed curve), $I(A:B)$ (red dot-dashed curve).

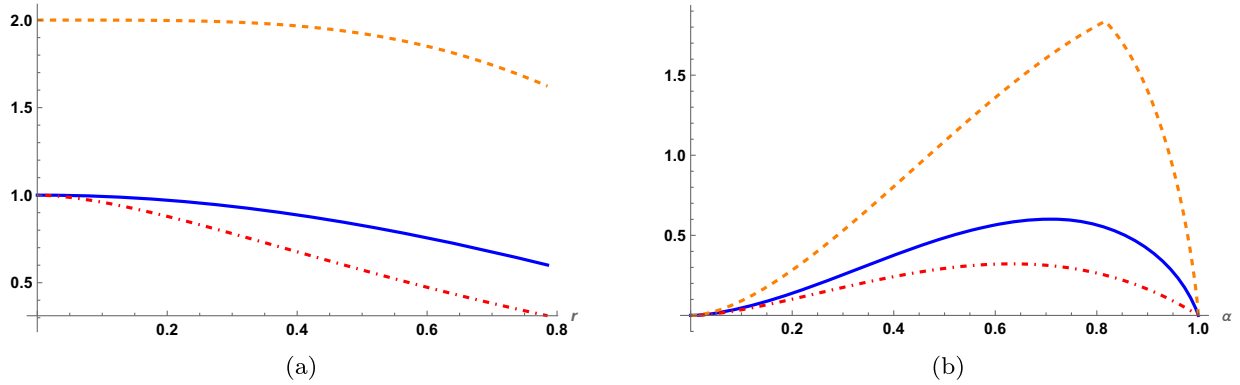

FIG. 6. (a) The reflected entropy $S_R(A:B)$ for the maximally entangled GHZ state as function of r is compared with its upper and lower bounds. (b) Reflected entropy $S_R(A:B)$ as a function of α for $r = \frac{\pi}{4}$ is compared with its upper and lower bounds. $S_R(A:B)$ (blue solid curve), $\min\{2S_A, 2S_B\}$ (orange dashed curve), $I(A:B)$ (red dot-dashed curve). $S_R(A:B)$ (blue solid curve), $\min\{2S_A, 2S_B\}$ (orange dashed curve), $I(A:B)$ (red dot-dashed curve).

IV. MARKOV GAP

In this section, we will study the Markov gap h which is proposed as a measure of tripartite entanglement [8]. For a bipartite system $A \cup B$, it is defined as the difference between reflected entropy and mutual information [6,21,34]

$$h(A:B) = S_R(A:B) - I(A:B). \tag{4.1}$$

This quantity is identified with conditional mutual information [10]

$$h(A:B) = I(A:B^\star|B) = I(B:A^\star|A), \tag{4.2}$$

where the conditional mutual information is defined in terms of the linear combination of entanglement entropies as follows:

$$\begin{aligned} I(A:C|B) &= S(AB) + S(BC) - S(ABC) - S(B) \\ &= I(A:BC) - I(A:B). \end{aligned} \tag{4.3}$$

The fidelity of a Markov recovery process is related to the conditional mutual information as [35]

$$\max_{\mathcal{R}_{B\to BC}} F(\rho_{ABC}, \mathcal{R}_{B\to BC}(\rho_{AB})) \geq \exp^{-I(A:C|B)}. \tag{4.4}$$

Here the Markov recovery process is understood as a technique to obtain the state ρ_{ABC} from any of its bipartite reduced states using Markov recovery map $\mathcal{R}_{B\to BC}$.[4] The quantity F in Eq. (4.4) is known as quantum fidelity, which for two density matrices ρ and σ is defined as

$$F(\rho,\sigma) = \left[\mathrm{Tr}\sqrt{\sqrt{\rho}\sigma\sqrt{\rho}}\right]^2. \tag{4.5}$$

Note that it is symmetric in its arguments which lie in the range $0 \leq F(\rho,\sigma) \leq 1$. Utilizing the canonically purified state $\rho_{ABA^\star B^\star}$, an inequality can be proposed as [21]

[4]The Markov recovery map essentially is a quantum channel which produces a bipartite system from a single-party system.

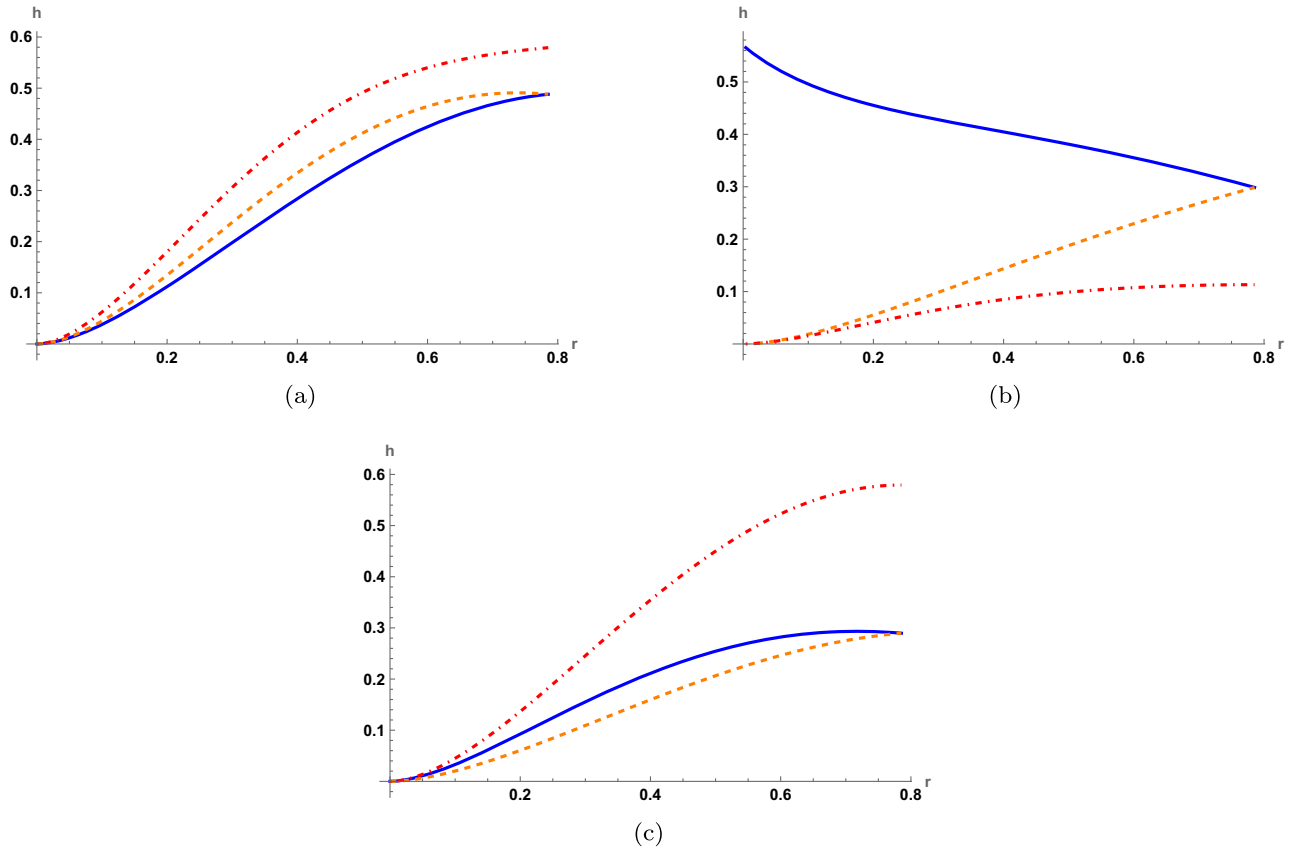

FIG. 7. Markov gap for the Bell, Werner, and GHZ states are plotted as a function of the acceleration. (a) Bell state: $h(A:B)$ (blue solid curve), $h(A:\bar{B})$ (orange dashed curve), and $h(B:\bar{B})$ (red dot-dashed curve). (b) Werner state: $h(A:B)$ (blue solid curve), $h(A:\bar{B})$ (orange dashed curve), and $h(B:\bar{B})$ (red dot-dashed curve). (c) GHZ state: $h(A:B)$ (blue solid curve), $h(A:\bar{B})$ (orange dashed curve), and $h(B:\bar{B})$ (red dot-dashed curve).

$$h(A:B) \geq -\max_{\mathcal{R}_{B\to BB^\star}} \log F(\rho_{ABB^\star}, \mathcal{R}_{B\to BB^\star}(\rho_{AB})), \quad (4.6)$$

where Eqs. (4.2) and (4.4) are used to obtain the above equation.

Markov gap can be studied in the present setup of this article where we investigate three-party (Alice-Bob–anti-Bob) entanglement for the Bell, Werner, and GHZ states in noninertial frame. The characteristic behavior of the Markov gap $h(A:B)$, $h(A:\bar{B})$, and $h(B:\bar{B})$ as a function of the acceleration r for a constant α is depicted in Fig. 7. Interestingly, we observe that the Markov gap for all three cases increases monotonically for the Bell state [Fig. 7(a)] and GHZ state [Fig. 7(c)], whereas for the W state, $h(A:B)$ decreases but $h(A:\bar{B})$ and $h(B:\bar{B})$ increase monotonically [Fig. 7(b)].

These figures indicate a few characteristics of multipartite entanglement in these three states. For the Bell state, the entanglement is purely bipartite at $r = 0$, and consequently the Markov gap vanishes. Anti-Bob $(\bar{B})$ evolves with increasing acceleration which creates tripartite correlation in the system. As a result, the Markov gaps $h(A:B)$, $h(A:\bar{B})$, and $h(B:\bar{B})$ increase with the acceleration. Interestingly, the authors in [3] studied the evolution of three-party correlation by exploring a measure named residual tangle [19]. Their system under consideration was the same as the first case in this article, i.e., the Bell state with accelerating Bob. It was found that the residual tangle is zero for any value of acceleration. This result was interpreted as the absence of tripartite correlation where all the entanglement present in the system is bipartite in nature. As the Markov gap is sensitive toward the tripartite entanglement, our results can be interpreted as the presence of three-party entanglement in the Bell state under acceleration even if the residual tangle vanishes. This behavior of the Markov gap suggests that it might be able to serve as a fine probe of multipartite entanglement.

Interestingly, on the other hand, the W state has tripartite entanglement between Alice, Bob, and anti-Bob in the inertial frame ($r = 0$), which is indicated by the nonzero initial value of $h(A:B)$. Furthermore, anti-Bob does not exist in the inertial frame where the Markov gap related to him is zero. The Markov gap $h(A:B)$ shows a monotonic decreasing behavior because of the entanglement sharing

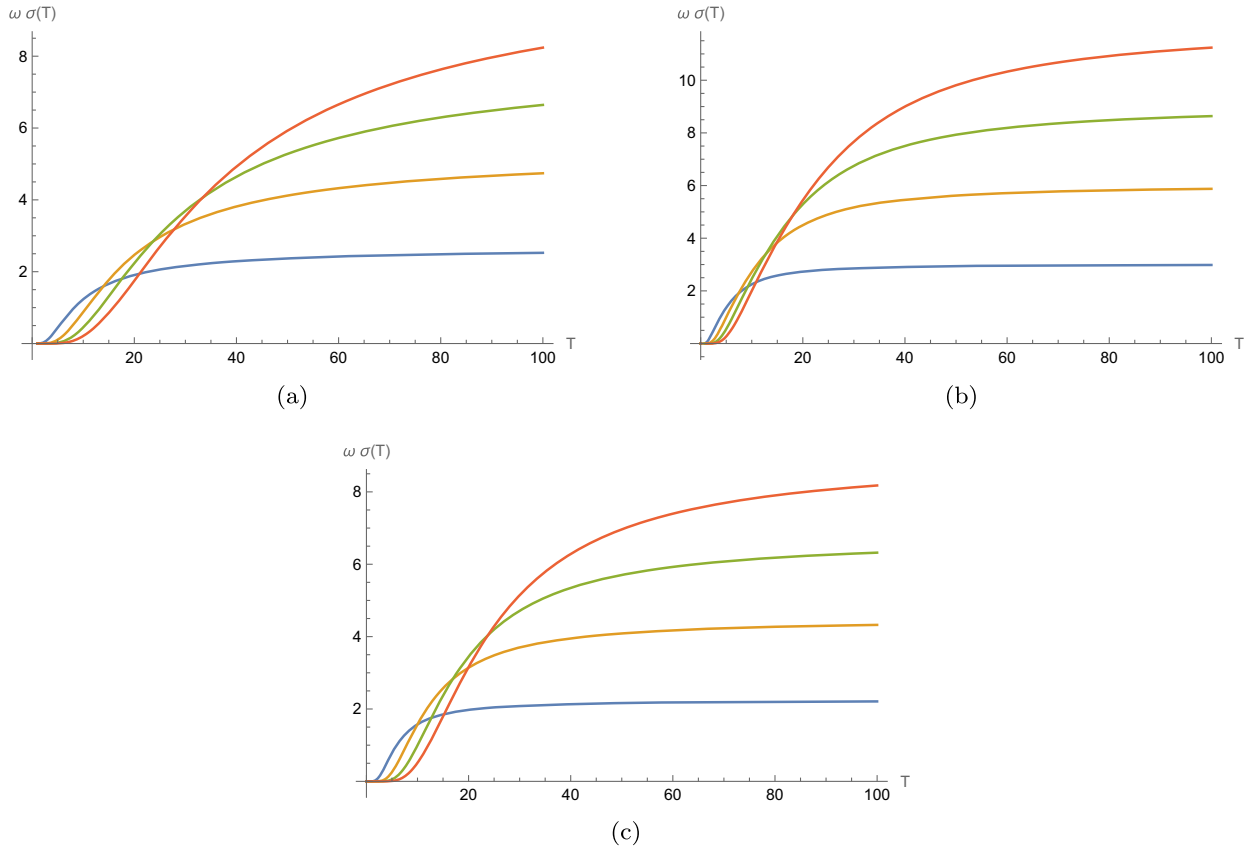

FIG. 8. $\omega \cdot \sigma(T)$ as function of the Unruh temperature T. (a) Bell state: $\omega = 10$ (blue), $\omega = 20$ (orange), $\omega = 30$ (green), and $\omega = 40$ (red). (b) Werner state: $\omega = 10$ (blue), $\omega = 20$ (orange), $\omega = 30$ (green), and $\omega = 40$ (red). (c) GHZ state: $\omega = 10$ (blue), $\omega = 20$ (orange), $\omega = 30$ (green), and $\omega = 40$ (red).

between Alice, Bob, and anti-Bob with increasing acceleration. Note that at $r = \frac{\pi}{4}$, the Markov gap $h(A:B)$ coincides with $h(A:\bar{B})$ similar to other findings in this article and in [3]. Furthermore, for the GHZ states, $h(A:B)$, $h(A:\bar{B})$, and $h(B:\bar{B})$ increase monotonically as function of r starting from zero at $r = 0$. The nature of the tripartite entanglement computed by the Markov gap for the GHZ state is similar to that of the Bell state with accelerating Bob as depicted in Fig. 7(c).

V. A MONOTONIC FUNCTION FOR REFLECTED ENTROPY

In this section, we will study a few properties of reflected entropy in our setup by defining a specific function of the temperature and frequency. Here we use the relation between the acceleration and the Unruh temperature

$$r = \tan^{-1}(e^{-\frac{\omega}{2T}}) \tag{5.1}$$

to obtain the characteristics of reflected entropy with respect to the Unruh temperature T. We find that for fixed ω and increasing T all the maximally entangled states have a monotonically decreasing behavior of $S_R(A:B)$ and $I(A:B)$ with T. We also notice that the dimensionless, single parameter function $\sigma(T)$, which we define as

$$\sigma(T) = \frac{1}{\omega}\frac{\partial S_R}{\partial(\frac{1}{T})}, \tag{5.2}$$

where ω can be considered as the fixed scale, has monotonic properties with respect to the increase of the temperature. In Figs. 8(a)–8(c), we observe $\sigma(T)$ increases monotonically with increasing Unruh temperature, meaning that the entanglement measure S_R we are interested in decreases for increasing acceleration. The σ function tends to zero for $T \to 0$ and for $T \to \infty$ saturates to fixed values which are different for each state and independent of ω. Notice that the σ function does not suffer from divergences, and for our states, for two-party and three-party systems having bipartite, W- and GHZ-type entanglement, the generic behavior remains the same. We point out that the definition of this function is partly motivated by the well-known c function in terms of the entanglement entropy proposed and further studied in [36–40]. By establishing the monotonicity of the function, one may like to question whether there exists a clear physically relevant interpretation of the function in relation to the degrees

of freedom shared between the two parties. An initial approach is that observers with higher accelerations are further away from the origin, covering only a subspace of the observers with lower accelerations and therefore should be associated with fewer degrees of freedom. It is worthy to be studied in even more complex setups in order to obtain a more solid interpretation.

VI. SUMMARY AND DISCUSSION

In this paper, we have investigated the behavior of reflected entropy between two modes of free fermionic fields in a noninertial frame from the perspective of two relatively accelerated observers. Alice and Bob, for a bipartite system described by the Bell state, and we added Charlie for the tripartite system represented by the Werner and GHZ states. We have confirmed that for our three-qubit and four-qubit states, Renyi reflected entropy is monotonic under partial trace, allowing us to use reflected entropy as a legitimate measure of correlation. This is an essential check since recent developments raised concerns about the generic validity and applicability of the reflected entropy as a correlation measure in quantum information theory [22] by pointing out the existence of a fine-tuned state that violates the desirable monotonicity. In fact, we have validated these developments by showing that such fine-tuned states can exist in higher-dimensional Hilbert spaces, and we have explicitly presented a class of such states. Nevertheless, getting back to our setup and our used states in this work, we have confirmed that the reflected entropy does reduce under the partial tracing of the degrees of freedom.

We have shown that the reflected entropy between Alice and Bob degrades with acceleration due to the Unruh effect, culminating in a nonvanishing minimum value. We have also computed the reflected entropy between Alice and anti-Bob (who is causally separated from the observer Bob in region I) and Bob and anti-Bob. We have discovered that the reflected entropy increases monotonically with acceleration in these two circumstances. Furthermore, we have explored the Markov gap, which is a measure of tripartite entanglement, between all three parties Alice-Bob, Alice–anti-Bob, and Bob–anti-Bob. We have found that the Markov gap increases monotonically with acceleration in all three scenarios for the Bell and GHZ states, whereas for the W state it declines for Alice-Bob but grows for Alice–anti-Bob, and Bob–anti-Bob. In the Bell and GHZ states, for vanishing acceleration, the Markov gap was zero. We have argued that acceleration causes tripartite entanglement in the system for all three states in consideration, as evidenced by the nonzero value of the Markov gap at finite and even infinite acceleration in Figs. 7(a)–7(c). This observation suggests that the Markov gap could be used to characterize the three-body correlation encoded for tripartite states apart from some other measures in the literature.

We have suggested a dimensionless σ function of reflected entropy for a fixed mode frequency which preserves monotonicity with increasing temperature. Because of the character of the reflected entropy, this specific function is free from any divergences. The function exhibits always a convergence to certain values at $T \to 0$ and $T \to \infty$. We suggest the possibility that this function contains information of the effective degrees of freedom or the shared correlation between two parties.

As for future direction, it would be interesting to ask what happens if Alice and Bob both accelerate simultaneously with different rates of acceleration. Intuitively, one could expect that reflected entropy between Alice and Bob to further decrease, eventually reaching a nonzero value in the infinite acceleration limit. Another interesting path for future research along this line is to address the same question for black hole spacetimes. In addition, it will be exciting to check the generalized properties of the σ function independent of the choices of states.

ACKNOWLEDGMENTS

The authors are grateful to V. Malvimat for useful discussions. D. G. would like to thank the Department of Theoretical Physics of CERN and the University of Cyprus, for hospitality during the final stages of this work. The research work of J. K. B. is supported by the National Science and Technology Council of Taiwan with Grant No. 112-2636-M-110-006. The research work of D. G. is supported by the National Science and Technology Council (NSTC) of Taiwan with the Young Scholar Columbus Fellowship Grant No. 112-2636-M-110-006. This research work of S. M. and W. Y. W. is supported in part by the Taiwan's NSTC Grant No. 109-2112-M-033-005-MY3 and the National Center for Theoretical Sciences.

APPENDIX A: THE DENSITY OF MATRICES OF THE BELL STATE

The density matrices $\rho_{AB}^{(B)}$, $\rho_{A\bar{B}}^{(B)}$, and $\rho_{B\bar{B}}^{(B)}$ for the Bell state have been given in section II A. Using a proper basis $\{|00\rangle, |01\rangle, |10\rangle, |11\rangle\}$, $\rho_{AA^\star} = \mathrm{Tr}_{BB^\star}(|\sqrt{\rho_{ABA^\star B^\star}}\rangle\langle\sqrt{\rho_{ABA^\star B^\star}}|)$, $\bar{\rho}_{AA^\star} = \mathrm{Tr}_{B\overline{B^\star}}(|\sqrt{\rho_{A\bar{B}A^\star\overline{B^\star}}}\rangle\langle\sqrt{\rho_{A\bar{B}A^\star\overline{B^\star}}}|)$, and $\rho_{BB^\star} = \mathrm{Tr}_{\bar{B}\,\overline{B^\star}}(|\sqrt{\rho_{B\bar{B}B^\star\overline{B^\star}}}\rangle\langle\sqrt{\rho_{B\bar{B}B^\star\overline{B^\star}}}|)$ are given as follows:

$$\begin{pmatrix} \frac{\alpha^2((2\alpha^2-1)\cos 2r+1)}{-\alpha^2+\alpha^2\cos 2r+2} & 0 & 0 & -\frac{\sqrt{2}\alpha^2(\alpha^2-1)\sin^2 r}{\sqrt{\alpha^2\sin^2 r(-\alpha^2+\alpha^2\cos 2r+2)}} \\ 0 & -\frac{2\alpha^2(\alpha^2-1)\cos^2 r}{-\alpha^2+\alpha^2\cos 2r+2} & 0 & 0 \\ 0 & 0 & -\frac{2\alpha^2(\alpha^2-1)\cos^2 r}{-\alpha^2+\alpha^2\cos 2r+2} & 0 \\ -\frac{\sqrt{2}\alpha^2(\alpha^2-1)\sin^2 r}{\sqrt{\alpha^2\sin^2 r(-\alpha^2+\alpha^2\cos 2r+2)}} & 0 & 0 & \frac{2(\alpha^2-1)^2}{-\alpha^2+\alpha^2\cos 2r+2} \end{pmatrix}, \tag{A1}$$

$$\begin{pmatrix} \frac{\alpha^2((2\alpha^2-1)\cos(2r)-1)}{\alpha^2+\alpha^2\cos(2r)-2} & 0 & 0 & -\frac{\alpha(\alpha^2-1)\cos(r)}{\sqrt{1-\alpha^2\cos^2(r)}} \\ 0 & \frac{2\alpha^2(\alpha^2-1)\sin^2(r)}{\alpha^2+\alpha^2\cos(2r)-2} & 0 & 0 \\ 0 & 0 & \frac{2\alpha^2(\alpha^2-1)\sin^2(r)}{\alpha^2+\alpha^2\cos(2r)-2} & 0 \\ -\frac{\alpha(\alpha^2-1)\cos(r)}{\sqrt{1-\alpha^2\cos^2(r)}} & 0 & 0 & -\frac{2(\alpha^2-1)^2}{\alpha^2+\alpha^2\cos(2r)-2} \end{pmatrix}, \tag{A2}$$

$$\begin{pmatrix} \alpha^2\cos^4(r) & 0 & 0 & \alpha\sqrt{1-\alpha^2}\cos^2(r) \\ 0 & \alpha^2\sin^2(r)\cos^2(r) & 0 & 0 \\ 0 & 0 & \alpha^2\sin^2(r)\cos^2(r) & 0 \\ \alpha\sqrt{1-\alpha^2}\cos^2(r) & 0 & 0 & -\alpha^2+\alpha^2\sin^2(r)\cos^2(r)+1 \end{pmatrix}. \tag{A3}$$

The reflected entropy $S_R(A:B)$, $S_R(A:\bar{B})$, and $S_R(B:\bar{B})$ may be obtained by employing Eq. (3.7) and using the information above. The expression of these density matrices ρ_{AA^*}, $\bar{\rho}_{AA^*}$, and ρ_{BB^*} for the W state and GHZ state are large, and we have not included them here for presentation reasons.

APPENDIX B: POLYGAMY INEQUALITY

To show the polygamy inequality Eq. (3.9), we construct $S_R(A:B)+S_R(A:\bar{B})-S_R(A:B\bar{B})$ for the Bell state and $S_R(A:B)+S_R(A:\bar{B}C)-S_R(A:B\bar{B}C)$ for the Werner and GHZ states for fixed α and plot these in Figs. 9(a)–9(c). We notice that for the Bell and GHZ states, it increases monotonically with growing r and remains positive for all values of r; thus, it satisfies the polygamy inequality. Unlike the Bell and GHZ states, for the W state it decreases monotonically with r from a maximum value at $r=0$, although it satisfies the polygamy inequality as it remains positive for all r.

APPENDIX C: MONOTONICITY OF REFLECTED ENTROPY

In this section, we show some representative plots of the monotonicity of the reflected entropy by depicting $S_R^{(\xi)}(A:B\bar{B})-S_R^{(\xi)}(A:B)$ as a function of the Renyi index ξ for the Bell, Werner, and GHZ states. We show that $S_R^{(\xi)}(A:B\bar{B})-S_R^{(\xi)}(A:B)$ is always positive for any value of ξ, which indicates that the reflected entropy (Renyi index $\xi=1$) is a valid correlation measure for the systems under question. We have considered all the possible configurations of the parties to check the monotonicity, where in Fig. 10 only three representatives have been presented.

Nevertheless, here we further elaborate on the existence of other generic quantum states that violate the

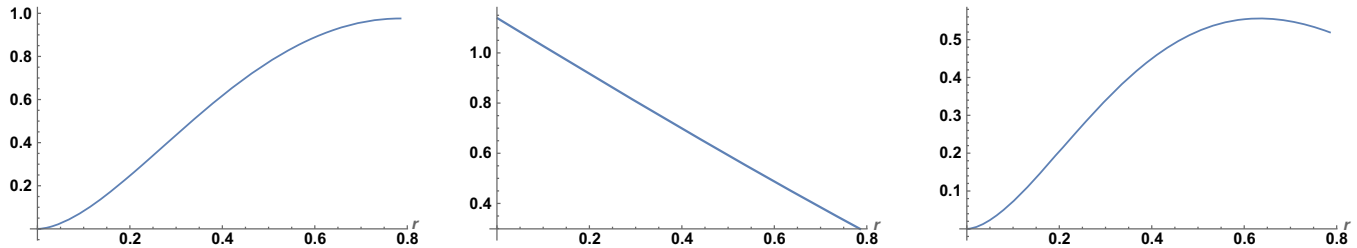

FIG. 9. Polygamy inequality as function of the acceleration. (a) Bell state. (b) W state. (c) GHZ state.

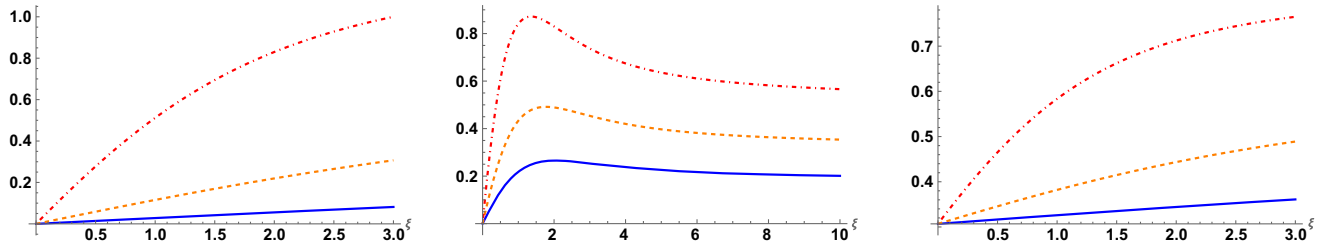

FIG. 10. $S_R^{(\xi)}(A:B\bar{B}) - S_R^{(\xi)}(A:B)$ are plotted as a function of the Renyi index ξ for $r = \frac{\pi}{16}$ (solid blue), $r = \frac{\pi}{8}$ (orange dashed), and $r = \frac{\pi}{4}$ (red dot-dashed). (a) Bell state. (b) W state. (c) GHZ state.

monotonicity of the reflected entropy under partial trace, and we find new generalized states with this property in higher-dimensional Hilbert spaces. The violation depends on the ratio $p = \frac{a}{b}$, which changes with the dimension of the Hilbert space. Such a generic state in $\mathcal{H}_A \otimes \mathcal{H}_B \otimes \mathcal{H}_C = \mathbb{C}^{n+1} \otimes \mathbb{C}^{m+1} \otimes \mathbb{C}^2$ can be suggested to be

$$\rho_{ABC} = \frac{1}{2na + 2(m-1)b}\Big[a|000\rangle\langle 000| + a|110\rangle\langle 110| + \sum_{m,n}(a|n00\rangle\langle n00| + a|n10\rangle\langle n10|) + b|0m0\rangle\langle 0m0| + b|1m1\rangle\langle 1m1|)\Big], \tag{C1}$$

where n, $m \geq 2$. Considering $n = m = 2$, we get the states given in [22]. The state presented in Eq. (3.11) can be reproduced by taking $n = 3$ and $m = 2$ in Eq. (C1). We expect that for any arbitrary value of m and n, the plots for $S_R^{\xi}(A:BC) - S_R^{\xi}(A:B)$ with respect to the Renyi index and p are similar to those presented in Figs. 3(a) and 3(b). The generic state in Eq. (C1) represents the class of states showing the nonmonotonicity of the reflected entropy. It would be interesting to study the characteristics of these states in detail compared to the states that respect the monotonicity under partial tracing.

[1] I. Fuentes-Schuller and R. B. Mann, Alice falls into a black hole: Entanglement in non-inertial frames, Phys. Rev. Lett. **95**, 120404 (2005).
[2] D. Walls and G. Milburn, *Quantum Optics* (Springer, Berlin, 2008).
[3] P. M. Alsing, I. Fuentes-Schuller, R. B. Mann, and T. E. Tessier, Entanglement of Dirac fields in non-inertial frames, Phys. Rev. A **74**, 032326 (2006).
[4] P. C. W. Davies, Scalar production in Schwarzschild and Rindler metrics, J. Phys. A **8**, 609 (1975).
[5] W. G. Unruh, Notes on black-hole evaporation, Phys. Rev. D **14**, 870 (1976).
[6] Y. Liu, Y. Kusuki, J. Kudler-Flam, R. Sohal, and S. Ryu, Multipartite entanglement in two-dimensional chiral topological liquids, arXiv:2301.07130.
[7] Y. Liu, R. Sohal, J. Kudler-Flam, and S. Ryu, Multipartitioning topological phases by vertex states and quantum entanglement, Phys. Rev. B **105**, 115107 (2022).
[8] Y. Zou, K. Siva, T. Soejima, R. S. K. Mong, and M. P. Zaletel, Universal tripartite entanglement in one-dimensional many-body systems, Phys. Rev. Lett. **126**, 120501 (2021).
[9] I. H. Kim, B. Shi, K. Kato, and V. V. Albert, Chiral central charge from a single bulk wave function, Phys. Rev. Lett. **128**, 176402 (2022).
[10] S. Dutta and T. Faulkner, A canonical purification for the entanglement wedge cross-section, J. High Energy Phys. 03 (2021) 178.
[11] P. Bueno and H. Casini, Reflected entropy for free scalars, J. High Energy Phys. 11 (2020) 148.
[12] P. Bueno and H. Casini, Reflected entropy, symmetries and free fermions, J. High Energy Phys. 05 (2020) 103.
[13] S. Dutta, T. Faulkner, and S. Lin, The reflected entanglement spectrum for free fermions, J. High Energy Phys. 02 (2023) 223.
[14] R. Sohal and S. Ryu, Entanglement in tripartitions of topological orders: A diagrammatic approach, Phys. Rev. B **108**, 045104 (2023).
[15] C. Berthiere, H. Chen, Y. Liu, and B. Chen, Topological reflected entropy in Chern-Simons theories, Phys. Rev. B **103**, 035149 (2021).
[16] T. Takayanagi and K. Umemoto, Entanglement of purification through holographic duality, Nat. Phys. **14**, 573 (2018).

[17] K. Umemoto and Y. Zhou, Entanglement of purification for multipartite states and its holographic dual, J. High Energy Phys. 10 (2018) 152.
[18] C. Akers and P. Rath, Entanglement wedge cross sections require tripartite entanglement, J. High Energy Phys. 04 (2020) 208.
[19] V. Coffman, J. Kundu, and W. K. Wootters, Distributed entanglement, Phys. Rev. A **61**, 052306 (2000).
[20] Y.-C. Ou and H. Fan, Monogamy inequality in terms of negativity for three-qubit states, Phys. Rev. A **75**, 062308 (2007).
[21] P. Hayden, O. Parrikar, and J. Sorce, The Markov gap for geometric reflected entropy, J. High Energy Phys. 10 (2021) 047.
[22] P. Hayden, M. Lemm, and J. Sorce, Reflected entropy is not a correlation measure, Phys. Rev. A **107**, L050401 (2023).
[23] M. Soffel, B. Müller, and W. Greiner, Dirac particles in Rindler space, Phys. Rev. D **22**, 1935 (1980).
[24] W. Greiner, B. Müller, and J. Rafelski, *Quantum Electrodynamics of Strong Fields: With an Introduction into Modern Relativistic Quantum Mechanics*, Springer Series in Computational Physics (Springer-Verlag, Berlin, 1985).
[25] S. Takagi, Vacuum noise and stress induced by uniform acceleration: Hawking-Unruh effect in Rindler manifold of arbitrary dimension, Prog. Theor. Phys. Suppl. **88**, 1 (1986).
[26] R. Jáuregui, M. Torres, and S. Hacyan, Dirac vacuum: Acceleration and external-field effects, Phys. Rev. D **43**, 3979 (1991).
[27] D. McMahon, P. M. Alsing, and P. Embid, The Dirac equation in Rindler space: A pedagogical introduction, arXiv: gr-qc/0601010.
[28] Y. Kusuki, J. Kudler-Flam, and S. Ryu, Derivation of holographic negativity in AdS_3/CFT_2, Phys. Rev. Lett. **123**, 131603 (2019).
[29] H.-S. Jeong, K.-Y. Kim, and M. Nishida, Reflected entropy and entanglement wedge cross section with the first order correction, J. High Energy Phys. 12 (2019) 170.
[30] Y. Kusuki and K. Tamaoka, Dynamics of entanglement wedge cross section from conformal field theories, Phys. Lett. B **814**, 136105 (2021).
[31] Y. Kusuki and K. Tamaoka, Entanglement wedge cross section from CFT: Dynamics of local operator quench, J. High Energy Phys. 02 (2020) 017.
[32] M. A. Nielsen and J. Kempe, Separable states are more disordered globally than locally, Phys. Rev. Lett. **86**, 5184 (2001).
[33] A. C. Wall, Maximin surfaces, and the strong subadditivity of the covariant holographic entanglement entropy, Classical Quantum Gravity **31**, 225007 (2014).
[34] K. Siva, Y. Zou, T. Soejima, R. S. K. Mong, and M. P. Zaletel, Universal tripartite entanglement signature of ungappable edge states, Phys. Rev. B **106**, L041107 (2022).
[35] O. Fawzi and R. Renner, Quantum conditional mutual information and approximate Markov chains, arXiv:1410.0664.
[36] H. Casini and M. Huerta, A finite entanglement entropy and the *c*-theorem, Phys. Lett. B **600**, 142 (2004).
[37] H. Casini and M. Huerta, A *c*-theorem for the entanglement entropy, J. Phys. A **40**, 7031 (2007).
[38] S. Ryu and T. Takayanagi, Aspects of holographic entanglement entropy, J. High Energy Phys. 08 (2006) 045.
[39] R. C. Myers and A. Singh, Comments on holographic entanglement entropy and RG flows, J. High Energy Phys. 04 (2012) 122.
[40] C.-S. Chu and D. Giataganas, *c*-theorem for anisotropic RG flows from holographic entanglement entropy, Phys. Rev. D **101**, 046007 (2020).